Iranian Journal of Hydrogen & Fuel Cell 2(2017) 125-138

Iranian Journal of Hydrogen & Fuel Cell

IJHFC

Journal homepage://ijhfc.irost.ir

Finite element simulation and ANFIS prediction of dimensional error effect on distribution of BPP/GDL contact pressure in a PEM fuel cell

Pouya Pashaie, Mohsen Shakeri*, Salman Nourouzi

Fuel Cell Research and Technology Group, Department of Mechanical Engineering, Babol Noshirvani University of Technology, Babol, Iran.

Article Information

Article History:

Received:
20 June 2017
Received in revised form:
05 Sep 2017
Accepted:
01 Oct 2017

Keywords

PEM fuel cell
ANFIS
Bipolar plate
GDL contact pressure
Dimensional error

Abstract

Distribution of contact pressure between the bipolar plate and gas diffusion layer considerably affect the performance of proton exchange membrane fuel cell. In this regard, an adaptive neuro-fuzzy inference system (ANFIS) is developed to predict the contact pressure distribution on the gas diffusion layer due to dimensional errors of the bipolar plate ribs in a proton exchange membrane fuel cell. Firstly, the main data set of input/ output vectors for training and testing of the ANFIS is prepared based on a finite element simulation of the contact between the bipolar plate and gas diffusion layer. An experimental procedure is used to validate the simulation results. Then, the ANFIS is developed and validated using the randomly selected data series for network testing. The applied ANFIS model has ten inputs made up of the dimensional errors of the bipolar plate ribs ($e_1 \dots e_{10}$). The standard deviation of contact pressure distribution (P_{std}) on the gas diffusion layer is the unique output of the ANFIS model. To select the best ANFIS model, the average errors of various architectures two different data series of training and testing of the main data set are calculated. Results indicated that the developed ANFIS has an acceptable performance in predicting the contact pressure distribution for the cited fuel cell model. The proposed integrated prediction model is feasible and effective for the dimensional tolerances considered. This method can reduce computing time and cost considering the acceptable accuracy of the obtained results, and can be used to analyze the effects of dimensional errors of bipolar plate on the performance of proton exchange membrane fuel cell.

1. Introduction

The use of renewable energy sources in order to reduce the consumption of fossil fuels is very important. Hydrogen is the most abundant element in nature and an appropriate alternative to fossil fuels for lowering emissions. Proton exchange membrane (PEM) fuel cells have received wide attentions as highly efficient

*Corresponding Author's Fax: +981132320570
E-mail address: shakeri@nit.ac.ir

doi:10.22104/ijhfc.2017.2288.1141

clean power sources that use hydrogen and oxygen to generate electricity, heat, and water [1]. PEM fuel cells have advantages such as low-temperature operation, high power density and quick startup that make them suitable for automotive and portable applications [2,3].

The bipolar plate (BPP) and membrane electrolyte assembly (MEA) are the main components of a typical PEM fuel cell and play significant roles in the system [4]. A typical MEA is composed of a gas diffusion layer (GDL), catalyst layer and polymer electrolyte membrane. Contact pressure distribution between the BPP and GDL is an important factor that affects the performance of a PEM fuel cell [5,6]. On one hand, interfacial contact resistance can be reduced inside the cell with a high BPP/GDL contact pressure [5, 7]. On the other hand, over compression of GDL may occur with large contact pressure which results in an increase of flow resistance [6, 8-10]. Furthermore, large contact pressure may seriously deform the MEA causing cell leakage and an internal short [11, 12]. Therefore, investigating the contact pressure distribution between BPP and GDL is necessary.

Moreover, dimensional errors of BPP are inevitable and lead to inappropriate GDL pressure distribution, resulting in a decrease of fuel cell performance [13, 14]. Controlling the dimensional errors of BPP to very low levels is costly. Hence, b it is necessary to investigate the effects of dimensional errors on the performance of PEM fuel cell and obtain suitable tolerance values to avoid unnecessary costs and maintain proper GDL pressure distribution.

To the best of the authors' knowledge, the dimensional errors of components of the PEM fuel cell have not yet received enough consideration. In this regard, the main objective of this study is to present a methodology based on finite element simulation (FES) and adaptive neuro-fuzzy inference system (ANFIS) to predict GDL pressure distribution due to the dimensional errors of BPP in a PEM fuel cell. First, the main data set of input/output vectors for training and testing of the ANFIS is prepared based on the finite element simulation of contact between BPP and GDL. An experimental procedure is used to validate the simulation results. Then, the ANFIS is developed and validated using the randomly selected data series for network testing. Finally, an integrated prediction model is developed to predict GDL pressure distribution in the whole range of dimensional tolerances.

2. Finite element analysis

Using the commercial code of ABAQUS, a parametric finite element model of BPP/GDL contact is developed as shown in Fig. 1. The sample graphite BPP model for the present study is illustrated in Fig. 1.a. The parametric model of BPP/GDL contact consists of a 2-D section of the sample BPP and GDL (Fig. 1.b). The parameters of the BPP/GDL finite element model are described in Table 1. The present model includes a bipolar plate and gas diffusion layer with an active area of 40×40 mm^2. Also, non-uniform BPP/GDL contact due to dimensional errors (e_1 … e_{10}) can be seen in Fig. 1.b. The real heights of the BPP ribs can be calculated by Equation 1 as follows:

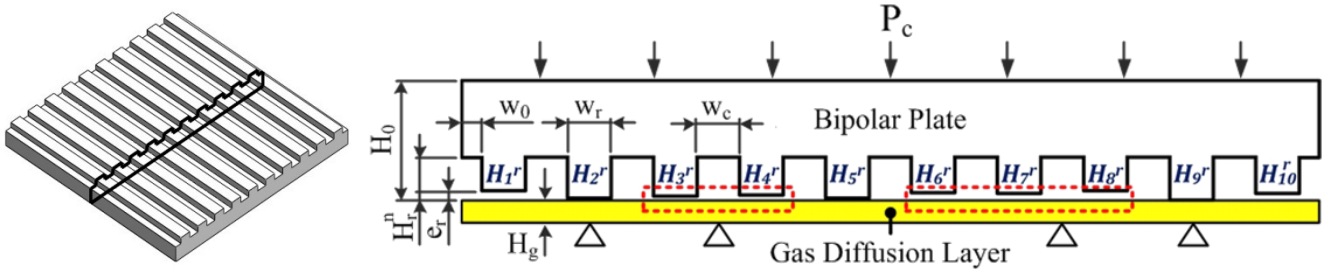

(a) (b)

Fig. 1. a) Sample graphite BPP model for the present study; b) Parametric model of BPP/GDL contact with exaggerated dimensional errors.

$$H_r^r = H_r^n + e_r \quad (1)$$

where H_r^r, H_r^n and e_r represent the real height, nominal height and dimensional error for ribr of BPP, respectively. The properties of materials used for finite element simulation are listed in Table 2.

Table 1. Parameters of the BPP/GDL finite element model.

Parameter	Value	Unit	Description
W_0	1	mm	width of BPP edges
W_r	2	mm	width of BPP ribs
W_c	2	mm	width of BPP channels
H_0	3	mm	overall height of BPP
H_r^n	1	mm	nominal height of BPP ribs
H_r^r	$1+e_r$	mm	real height of BPP ribs
H_g	0.25	mm	GDL thickness
P_c	0.5	MPa	clamping pressure

Meshing is very important to obtain an exact answer. In order for the contract model to achieve realistic physical behavior appropriate types of elements should be selected for each part and their contact surfaces. Finally, clamping load, boundary conditions and the contact properties of the components interfaces are properly defined and the finite element numerical model is solved. The number and type of the model meshing is shown in Table 3. The contact between BPP and GDL is selected as “surface to surface” of type “Finite sliding”. The normal behavior of contact is chosen as “hard contact” and the tangential behavior is set to “isotropic frictional”. Clamping pressure is also applied on the upper surface of BPP and displacement of the side surfaces of BPP is set to “Zero” in the X direction (U1). The displacement of the lower surface of GDL is set to “Zero” in the Y direction (U2), as well.

Meshing is very important to obtain an exact answer. In order for the contract model to achieve realistic physical behavior appropriate types of elements should be selected for each part and their contact surfaces. Finally, clamping load, boundary conditions and the contact properties of the components interfaces are properly defined and the finite element numerical model is solved. The number and type of the model meshing is shown in Table 3. The contact between BPP and GDL is selected as “surface to surface” of type “Finite sliding”. The normal behavior of contact is chosen as “hard contact” and the tangential behavior is set to “isotropic frictional”.

Various values of dimensional tolerances (from ± 0.01 mm to ± 0.1 mm at an interval of 0.01 mm) are applied on the parametric model and the BPP/GDL contact pressure values are calculated for the applied errors. Fig. 2 shows stress distribution in the BPP and GDL for an ideal model without dimensional errors (Fig. 2.a) compared to the model with ± 0.03 mm dimensional tolerance (Fig. 2.b). However, the amount of contact pressure (CPRESS) has been used to evaluate the performance of the fuel cell. For example, the distribution of contact pressure at the interface of the BPP/GDL for the ± 0.03 mm dimensional tolerance in comparison with the ideal model is presented in Fig. 3. As shown in Fig. 3, the dimensional error of BPP makes the BPP/GDL contact behavior non-uniform.

Table 2. Properties of materials used for finite element simulation.

Part	Material	Elastic modulus (MPa)	Poisson's ratio	Density ($g.cm^{-3}$)
BPP	graphite	13×103	0.1	1.83
GDL	Toray TGP-H-060	6.1	0.1	0.44

Table 3. The number and type of the model meshing.

Part	Number of nodes	Number of elements	Element type	Description
GDL	4806	4000	CPS4R	linear quadrilateral
BPP	2761	2500	CPS4R	linear quadrilateral
End Plate	1414	1300	CPS4R	linear quadrilateral
Total Model	8981	7800	CPS4R	linear quadrilateral

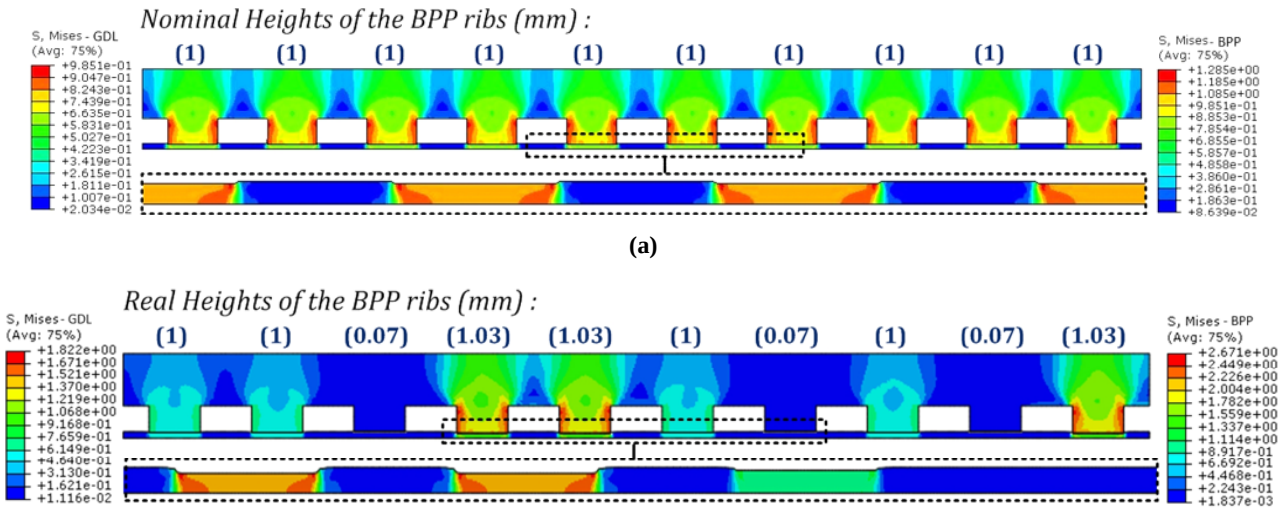

Fig. 2. Stress contour plot of the BPP and GDL a) Ideal model without dimensional error; b) Model with± 0.03 mm dimensional tolerance.

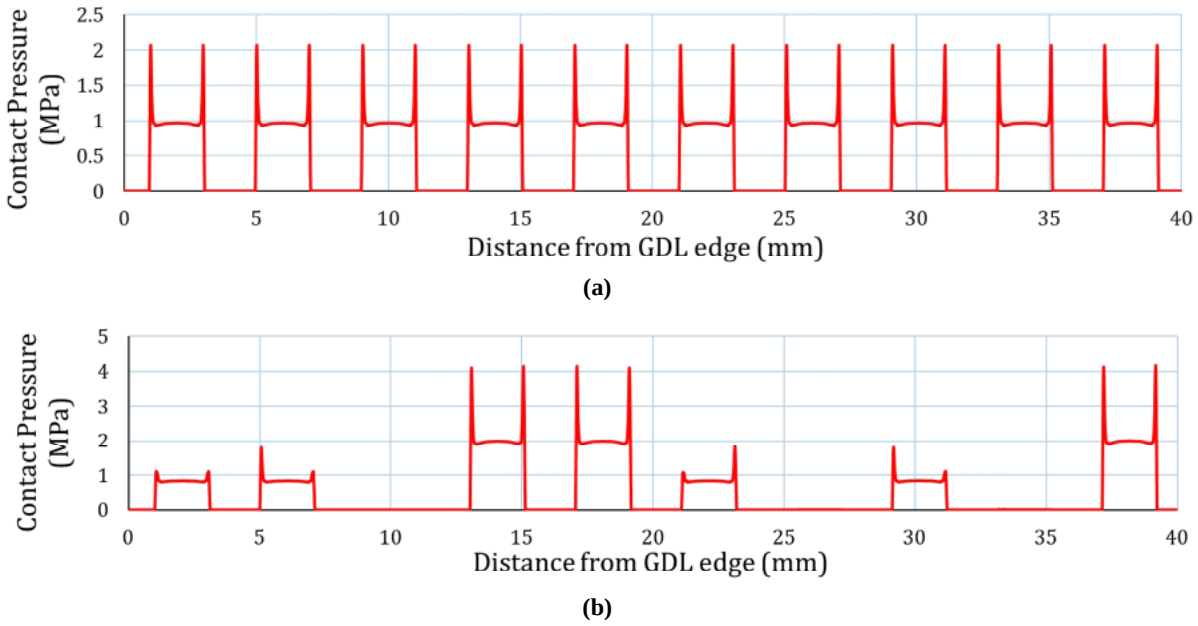

Fig. 3. Contact pressure distribution at the BPP/GDL interface a) Ideal model without dimensional error; b) Model with ±0.03 mm dimensional tolerance.

In this study, the mean Pave and standard deviation Pstd of the GDL contact pressure distribution are used to evaluate the PEM fuel cell performance. These values can be obtained with the parametric finite element model as follows:

$$P_{ave} = \frac{\sum_{i=1}^{n} P_i}{n} \quad (2)$$

$$P_{std} = \sqrt{\frac{\sum_{i=1}^{n} \left(P_i - P_{ave}\right)^2}{n}} \quad (3)$$

where P_i is the contact pressure of each contact element on the GDL and n is the number of all the contact elements on the GDL. If P_i exceeds yield strength (2.5 MPa), there will be residual stress in the GDL after unloading which influences the durability of the PEM. P_{ave} represents the average contact pressure and P_{std} represents the uniformity of the GDL contact pressure. When P_{ave} increases, it means that the contact behavior on the GDL becomes better. If P_{std} increases, it means that the uniformity

of pressure distribution becomes worse. Increasing the dimensional error has a significant effect on uniformity of the GDL pressure distribution (P_{std}), but has little effect on the mean contact pressure (P_{ave}). Also, stress concentration for some of the BPP ribs with dimensional error is the main reason that probability of GDL stress failure increases as the clamping force increases (Fig. 3-b).

3. Experimental study

The results of finite element simulations are validated through an experimental procedure. The experimental procedure has three main steps include manufacturing of BPP sample, evaluating BPP dimensional error using a laser scanning system, and experimentally examining the BPP/GDL contact pressure distribution under clamping pressure.

Initially, a sample BPP is fabricated with graphite sheet by a machining process (Fig. 4.a). The BPP sample has thickness of 3 mm with 10 parallel-channel flow fields. Then, the sample BPP is scanned by a laser measurement system. The obtained 3D CAD model of the sample is used to generate several 2D sections of BPP with real dimensions for the validation process. Also, TGP-H-060 carbon paper with a thickness of 0.25 mm and an active area of 40×40 mm^2 (Fig. 4.a) is used for the pressure distribution test.

Fig. 4.b schematically illustrates the facilities used for the GDL pressure test. In order to analyze the GDL pressure distribution, pressure sensitive film (PSF) from the FUJIFILM Company with a range of 0.5-2.5 MPa is inserted between the BPP and GDL. By increasing the contact pressure, the color of PSF slowly changes from white to red. Effect of PSF thickness on GDL contact pressure can be neglected according to the literatures [9, 15, 16].

Approximating the actual assemblyof a PEM fuel cell, the experiments are done under 0.5 MPa clamping pressure [13, 17]. In order to avoid deformation of the endplates, a press machine is used to set the compressive force. The clamping force is simultaneously applied at the speed of 1 mm/min. After 2 minutes, the assembly unit is unfixed and the pattern of GDL pressure distribution is formed on PSF. To check the repeatability, three replications are conducted for each case.

A sample result of the GDL pressure distribution test is shown in Fig. 5. The color profile of the PSF principally mirrored the pattern of BPP ribs. Based on the PSF calibration chart proposed by FUJIFILM Company, a MATLAB code is developed to transfer the color map into the contact pressure values. As shown in Fig. 5.a, different sections of PSF sample are considered to compare the results of the experimental test and finite element simulation. 2D profiles of the BPP sample in selected sections (Fig. 5.a) obtained from laser scanning are modeled in contact with GDL using the finite element solution described previously. Also, real contact pressure values are

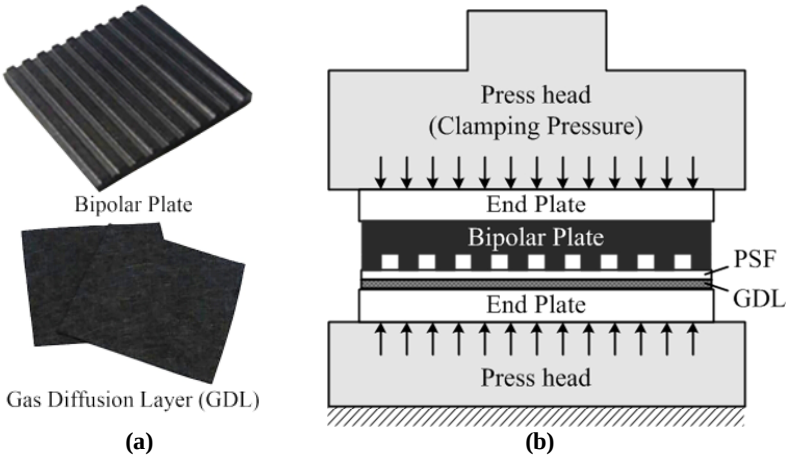

Fig. 4. a) Schematic diagram of the clamping pressure test; b) Bipolar plate and gas diffusion layer used for experimental validation.

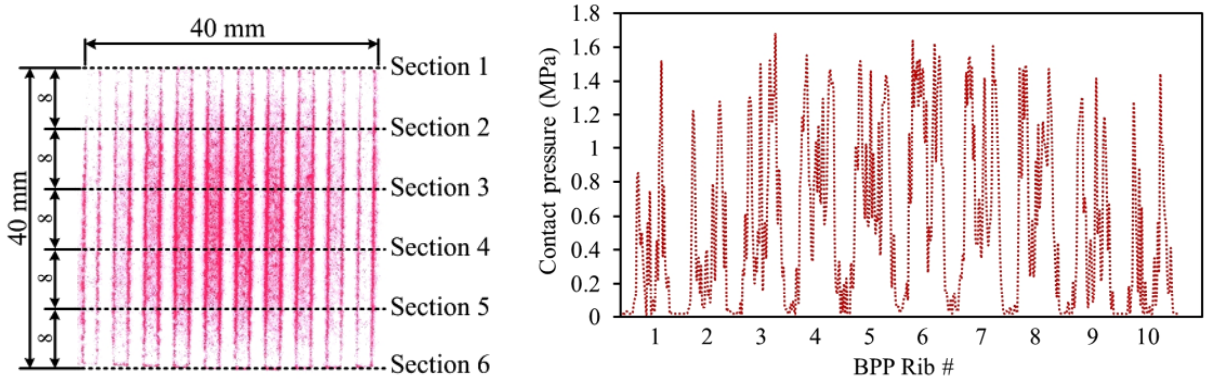

(a) (b)

Fig. 5. a) Pressure sensitive film from the experimental test and positions of calculated sections; b) Sample result obtained from PSF Calibration code in Section 3.

Table 4. BPP/GDL contact pressure values from finite element analysis and the experimental test

Section Number	average of contact pressure (MPa)		standard deviation of contact pressure (MPa)	
	finite element simulation	experimental test	finite element simulation	experimental test
1	0.9289	0.4653	0.3230	0.3234
2	0.9673	0.7410	0.3267	0.4146
3	0.9602	1.0051	0.3274	0.4806
4	0.9673	0.9628	0.3266	0.4655
5	0.9603	0.8368	0.3276	0.4362
6	0.9145	0.8746	0.3210	0.4447

calculated in each section of the PSF sample using MATLAB code. Fig. 5.b shows the result obtained from the Calibration code in Section 3 of the PSF sample. Finally, the results of finite element analysis can be compared with the experimental values as shown in Table 4. The results represents acceptable agreement of the solutions.

Although, it must be noticed that validation of the results is difficult due to other types of errors existing in the components. These errors would need more complicated models to simulate the BPP/GDL contact in a single cell and are not the focus of the present study.

4. Prediction model based on ANFIS

4.1. Adaptive neuro fuzzy inference system (ANFIS)

An ANFIS gives the mapping relationship between the input and output data using the hybrid learning method to determine the optimal distribution of membership functions [18]. Both artificial neural network and fuzzy logic are used in ANFIS architecture.

Basically, five layers are used to construct this inference system. Each ANFIS layer consists of several nodes described by the node function. The inputs of the present layers are obtained from the nodes in the previous layers. Fig. 6 shows the ANFIS structure for a system with m inputs ($X_1 \ldots X_m$), each with n membership functions (MFs), a fuzzy rule base of R rules and one output (Y). The network, consisting of five layers, is used for training the Sugeno-type fuzzy interface system (FIS) through learning and adaptation. The number of nodes (N) in layer 1 is the product of numbers of inputs (m) and MFs (n) for each input, i.e., N=mn. The number of nodes in layers 2-4 depends on the number of rules (R) in the fuzzy rule base.

The Fuzzification layer transforms the crisp inputs Xi to linguistic labels (Aij, like small, medium,

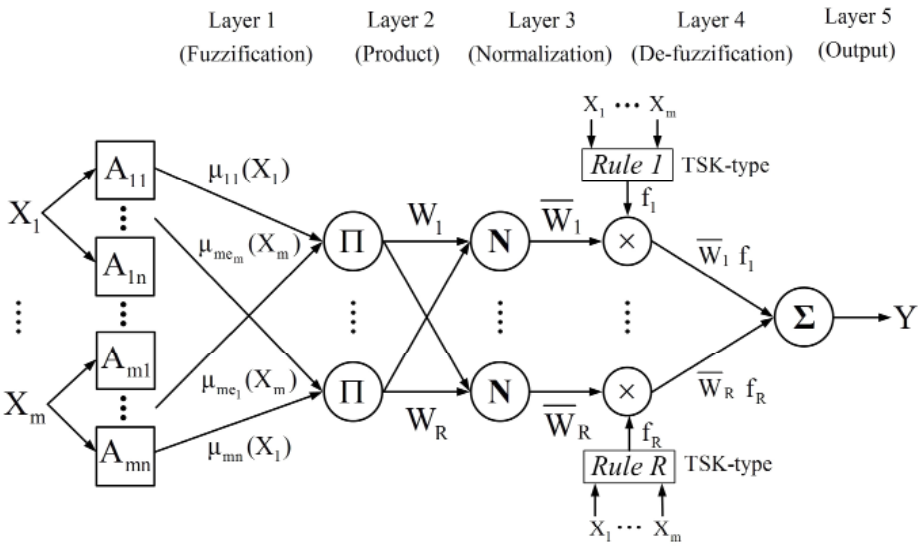

Fig. 6. Schematic of the ANFIS structure.

large, etc.) with a degree of membership. The output of node ij is expressed as follows:

$$O_{ij}^{1} = \mu_{ij}\left(X_i\right) \qquad i = 1\ldots m,\ j = 1\ldots n \tag{4}$$

where μ_{ij} is the j^{th} membership function for the input X_i. Several types of MFs can be used, for example triangular curve, generalized bell function, trapezoidal curve, Gaussian function and the sigmoidal function which are used in this study. The triangular curve is a function of a vector, x, and depends on three scalar parameters a, b, and c, as follows:

$$\mathrm{f}\left(\mathrm{x};\mathrm{a},\mathrm{b},\mathrm{c}\right) = \begin{Bmatrix} 0 & x \le a \\ x-a/b-a & a \le x \le b \\ c-x/c-b & b \le x \le c \\ 0 & c \le x \end{Bmatrix} \tag{5}$$

where a and c locate the "feet" of the triangle and the parameter b locates the peak. The generalized bell function depends on three parameters a, b, and c as follows:

$$\mathrm{f}\left(\mathrm{x};\mathrm{a},\mathrm{b},\mathrm{c}\right) = \frac{1}{1+\left|\dfrac{x-c}{a}\right|^{2b}} \tag{6}$$

where a and b vary the width of the curve and the parameter c locates the center of the curve. Also, b is usually positive. The trapezoidal curve is a function of a vector, x, and depends on four scalar parameters a, b, c, and d, as given by the following:

$$\mathrm{f}\left(\mathrm{x};\mathrm{a},\mathrm{b},\mathrm{c},\mathrm{d}\right) = \begin{Bmatrix} 0 & x \le a \\ x-a/b-a & a \le x \le b \\ 1 & b \le x \le c \\ d-x/d-c & c \le x \le d \\ 0 & d \le x \end{Bmatrix} \tag{7}$$

where the parameters a and d locate the "feet" of the trapezoid and the parameters b and c locate the "shoulders". The Gaussian function depends on two parameters σ and c as given by the following:

$$\mathrm{f}\left(\mathrm{x};\sigma,\mathrm{c}\right) = e^{\frac{-(x-c)^2}{2\sigma^2}} \tag{8}$$

where the parameter c locates the peak. The sigmoidal membership function is a mapping on the vector x, and depends on two parameters a and c as given in Equation 9. Depending on the sign of the parameter a, the sigmoidal membership function is inherently open to the right or to the left.

$$\mathrm{f}\left(\mathrm{x};\sigma,\mathrm{c}\right) = \frac{1}{1+e^{-a(x-c)}} \tag{9}$$

For each node k in the product layer, the output represents the weighting factor (firing strength) of

the rule k. The output Wk is the product of all its inputs as follows:

$$O_k^2 = \mathrm{W}_k = \mu_{1e_1}(X_1)\mu_{2e_2}(X_2)\ldots\mu_{3e_3}(X_m) \quad k = 1\ldots R;\quad e_1, e_2, \ldots, e_m = 1\ldots n \tag{10}$$

In the normalized layer, the output of each node k represents the normalized weighting factor W of the kth rule as follows:

$$\mathrm{O}_k^3 = \bar{W}_k = \frac{W_k}{W_1 + W_2 + \ldots + W_R} \tag{11}$$

Each node of the de-Fuzzification layer gives a weighted output of the first order TSK-type fuzzy if-then rule as follows:

$$\mathrm{O}_k^4 = \bar{W}_k f_k \tag{12}$$

where f_k represents the output of k^{th} TSK-type fuzzy rules as follows:

$$\textit{If } \left(X_1 \text{ is } A_{1e_1}\right) \text{ and} \left(X_{21} \text{ is } A_{2e_2}\right)\ldots\text{and} \left(X_m \text{ is } A_{me_m}\right) \quad \textit{Then } f_k = \sum_{i=1}^{m} p_{ie_i} X_i + r_k \tag{13}$$

where p_{ie1} and r_k are called consequent parameters.

The output layer is a single-node layer that represents the overall output (Y) of the network as the sum of all weighted outputs of the rules:

$$O^5 = Y = \sum_{k=1}^{n} \bar{W}_k f_k \tag{14}$$

4.2. ANFIS simulation process for dimensional error of BPP

The procedure of the ANFIS development for this study consists of three main steps including data set preparation, data pre-processing and developing the ANFIS network.

The main data set comprising 270 pairs of ten inputs (combination of dimensional errors of the BPP ribs) and one output (standard deviation of the GDL contact pressure) is prepared based on the already mentioned finite element analysis. A sample of this database is shown in Table 5. It is important to process the data set into patterns before the ANFIS can be trained and the mapping learnt. Training/testing pattern vectors are formed. Each pattern is formed with an input condition vector and the corresponding target vector [19, 20]. The scale of the input and output data is an important matter to consider, especially when the operating ranges of process parameters are different. The scaling or normalizing ensures that the ANFIS will be trained effectively, without any particular variable skewing the results significantly. As a result, all of the input parameters are equally important in the training of the network. The scaling is performed by mapping each term to a value between "0" and "1" using the following equation:

$$\mathrm{e}_{\mathrm{norm}} = \frac{\mathrm{e}_{\mathrm{i}} - \mathrm{e}_{\mathrm{min}}}{\mathrm{e}_{\mathrm{max}} - \mathrm{e}_{\mathrm{min}}} \tag{15}$$

where enorm is the normalized value of input error, e_i is the value of a certain variable ($e_1 \ldots e_{10}$) and e_{max} and e_{min}, respectively, are the maximum and minimum values of the independent dimensional error (with respect to the investigated dimensional tolerance of BPP ribs).

Then, the input pattern vectors are formed comprising 270 and 239 pairs of input/output , respectively, for training and testing the network on the basis of the main data set. The Testing data series is presented to the trained network as new application data for verifying or testing the predictive accuracy of the network model. Thus, the network is evaluated using data that have not been used for training.

The schematic structure of the developed ANFIS models is illustrated in Fig. 7. There are 10 inputs considered for the ANFIS model including the dimensional errors of BPP ribs and the only output of the model is the standard deviation of GDL contact pressure. After the structure is fixed, the performance of the model can be fine-tuned by adjusting its parameters. Defining fuzzy membership functions and corresponding values can be considered as an important stage in the modeling. The suitability of the architecture of the ANFIS is determined by trial and error. The Greed partitioning method is employed to partition the input space into a number of local

Table 5. Sample results of BPP/GDL contact simulation (±0.030 mm dimensional tolerance)

No.	Inputs : Dimensional Errors (mm)										Outputs : Contact Pressure	
	e_1	e_2	e_3	e_4	e_5	e_6	e_7	e_8	e_9	e_{10}	P_{ave} (MPa)	P_{std} (MPa)
1	0.03	0.03	0.03	0.03	0.03	0.03	0.03	0.03	0.03	0.03	0.8962	0.2120
2	0.03	0.03	0.03	0.03	0	0	0	0	0	0	0.9094	0.5159
3	0.03	0.03	0.03	0.03	-0.03	-0.03	-0.03	-0.03	-0.03	-0.03	0.9149	0.9318
4	0.03	0	0	0	0.03	0.03	0.03	0	0	0	0.9116	0.5758
5	0.03	0	0	0	0	0	0	-0.03	-0.03	-0.03	0.9114	0.6105
6	0.03	0	0	0	-0.03	-0.03	-0.03	0.03	0.03	0.03	0.9052	0.8017
7	0.03	-0.03	-0.03	-0.03	0.03	0.03	0.03	-0.03	-0.03	-0.03	0.9172	1.0632
8	0.03	-0.03	-0.03	-0.03	0	0	0	0.03	0.03	0.03	0.9092	0.8124
9	0.03	-0.03	-0.03	-0.03	-0.03	-0.03	-0.03	0	0	0	0.9143	0.8073
10	0	0.03	0	-0.03	0.03	0	-0.03	0.03	0	-0.03	0.9068	0.8195
11	0	0.03	0	-0.03	0	-0.03	0.03	0	-0.03	0.03	0.9068	0.8244
12	0	0.03	0	-0.03	-0.03	0.03	0	-0.03	0.03	0	0.9055	0.8243
13	0	0	-0.03	0.03	0.03	0	-0.03	0	-0.03	0.03	0.9071	0.8260
14	0	0	-0.03	0.03	0	-0.03	0.03	-0.03	0.03	0	0.9056	0.8191
15	0	0	-0.03	0.03	-0.03	0.03	0	0.03	0	-0.03	0.9053	0.8227
16	0	-0.03	0.03	0	0.03	0	-0.03	-0.03	0.03	0	0.9033	0.8232
17	0	-0.03	0.03	0	0	-0.03	0.03	0.03	0	-0.03	0.9054	0.8240
18	0	-0.03	0.03	0	-0.03	0.03	0	0	-0.03	0.03	0.9057	0.8219
19	-0.03	0.03	-0.03	0	0.03	-0.03	0	0.03	-0.03	0	0.9142	0.8989
20	-0.03	0.03	-0.03	0	0	0.03	-0.03	0	0.03	-0.03	0.9146	0.8985
21	-0.03	0.03	-0.03	0	-0.03	0	0.03	-0.03	0	0.03	0.9147	0.8902
22	-0.03	0	0.03	-0.03	0.03	-0.03	0	0	0.03	-0.03	0.9146	0.8988
23	-0.03	0	0.03	-0.03	0	0.03	-0.03	-0.03	0	0.03	0.9167	0.8983
24	-0.03	0	0.03	-0.03	-0.03	0	0.03	0.03	-0.03	0	0.9158	0.8955
25	-0.03	-0.03	0	0.03	0.03	-0.03	0	-0.03	0	0.03	0.9156	0.8932
26	-0.03	-0.03	0	0.03	0	0.03	-0.03	0.03	-0.03	0	0.9133	0.8916
27	-0.03	-0.03	0	0.03	-0.03	0	0.03	0	0.03	-0.03	0.9150	0.8841

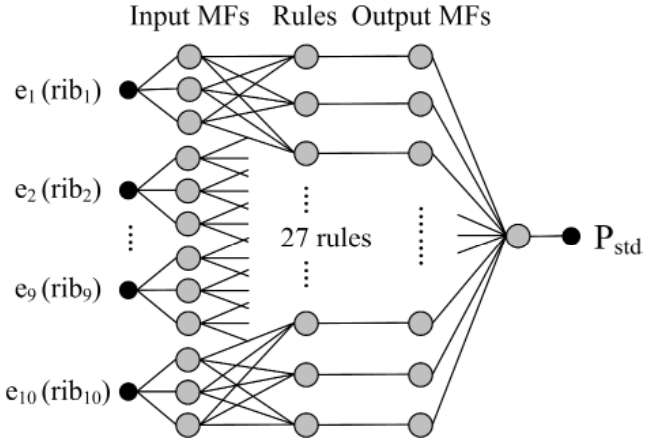

Fig. 7. Schematic structure of the developed ANFIS models

fuzzy regions and generate the Takagi-Suguno fuzzy inference system (FIS) structure. Different types of MFs are tested to generate the fuzzy inference system. Root mean square error (RMSE) is used to evaluate the results. The Gaussian membership functions demonstrated the best performances for the model (Fig. 8). For example, properties of the ANFIS model for ±0.01 mm dimensional tolerance is presented in Table 6.

4.3. Integrated prediction model

In order to predict the standard deviation values for BPP/GDL contact pressure distribution, a MATLAB code was used to integrate the ANFIS models developed for various dimensional tolerances. Fig.9 illustrates the main algorithm of the prediction code (integrated model). After the string of dimensional errors are given to the prediction network, a suitable ANFIS model is chosen based on the corresponding tolerance value. Then, the standard deviation of BPP/ GDL contact pressure can be properly predicted for the given error values (normalized inputs are used).

5. Evaluation of the predicted results

The testing data series is presented to the trained network as new application data for verifying or testing the predictive accuracy of the integrated

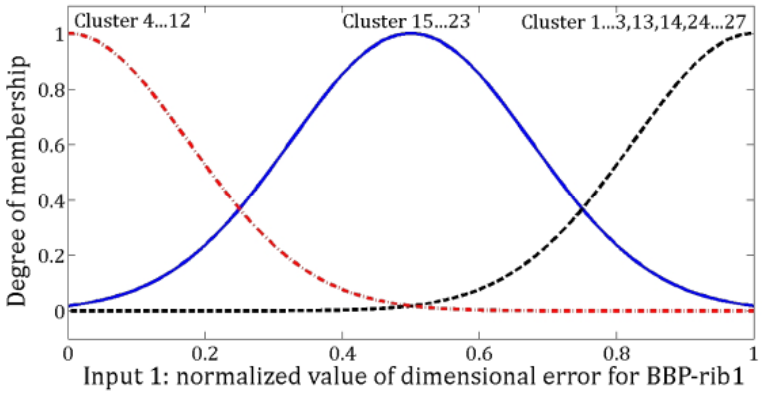

Fig. 8. Sample plot of membership function for inputs (dimensional errors of the BPP ribs).

Table 6. Properties of ANFIS model for ±0.01 mm dimensional tolerance

ANFIS model for ±0.01 mm dimensional tolerance	
Name of the Network	NET 1
Type of the Network	sugeno
Number of Inputs/Outputs	10 inputs and 1 output
Number of Input Membership Functions	27 (for each input)
Number of Output Membership Functions	27
Number of Rules	27
And Method	prod
Or Method	probor
ImpMethod	prod
AggMethod	sum
Defuzzification Method	wtaver
Input Ranges	[0 1]
Output Range	[0.212 0.4276]
Inputs Membership Functions Type	gaussmf
Output Membership Function Type	linear

prediction model. Thus, the network is evaluated using data that have not been used for training. Fig. 10 shows the results of testing the integrated prediction network with 239 random test pairs. These pairs are selected randomly in the range of investigated dimensional tolerances (±0.01 mm to ±0.1 mm at interval of 0.01 mm) and simulated using the already mentioned finite element method to determine Pstd (standard deviation of GDL pressure distribution). Also, the predicted values of Pstd for the same pairs of inputs are obtained using the integrated prediction code to compare the results. Table 7 represents obtained (finite element simulation) and predicted (ANFIS) values of Pstd (MPa) from the integrated neuro-fuzzy model together with percentage error as follows:

$$\text{Error}(\%) = \left|\frac{P_{FES} - P_{ANFIS}}{P_{FES}}\right| \times 100 \quad (16)$$

The regression line of the targets/outputs is shown in Fig. 11. It is indicated that assessed results have an acceptable accuracy in the specified range, and finite element simulation and ANFIS are feasible and effective for the study of dimensional error.

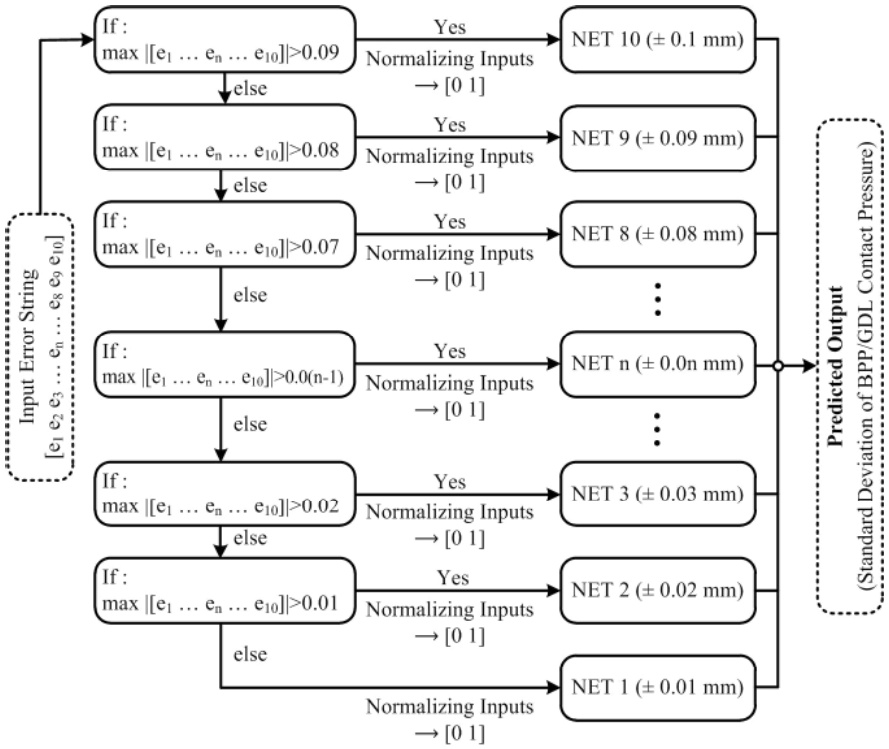

Fig. 9. The main model of BPP/GDL contact pressure prediction.

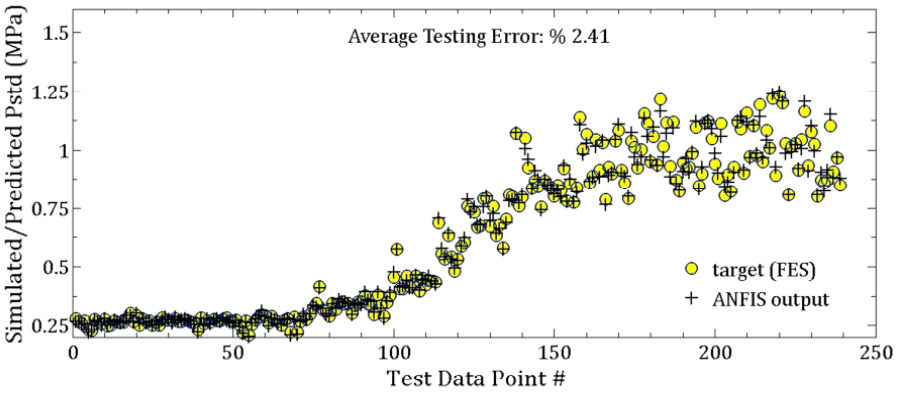

Fig. 10. Testing of the integrated prediction network with random test points.

Table 7. Obtained (FES) and predicted (ANFIS) values of Pstd (MPa) from the Integrated Neuro-Fuzzy Model together with Percentage Error.

No.	Inputs : Dimensional Errors (mm)										Output : Pstd (MPa)		Error (%)
	e_1	e_2	e_3	e_4	e_5	e_6	e_7	e_8	e_9	e_{10}	FES	ANFIS	
1	0.005	-0.002	0.001	-0.001	0.004	-0.003	-0.008	-0.003	-0.002	-0.001	0.280	0.266	4.823
2	-0.002	0.001	0.002	-0.004	0.004	-0.002	-0.003	0.000	-0.003	-0.005	0.265	0.265	0.041
3	-0.001	-0.002	-0.002	0.001	-0.002	-0.005	0.002	0.001	0.000	0.003	0.256	0.252	1.506
4	0.004	-0.004	-0.001	0.002	-0.001	0.005	-0.003	0.004	-0.002	-0.001	0.269	0.256	4.955
5	0.002	-0.001	0.003	-0.001	-0.003	0.002	0.003	0.003	0.000	0.001	0.230	0.222	3.208
6	0.003	0.004	-0.004	0.007	-0.002	0.005	0.001	0.001	-0.002	0.003	0.227	0.232	1.987
7	-0.001	-0.002	0.001	-0.001	-0.006	-0.002	-0.001	-0.001	-0.005	0.008	0.278	0.271	2.425
8	-0.004	0.006	0.001	-0.001	0.002	-0.005	0.002	-0.003	0.002	-0.001	0.266	0.263	1.320
9	-0.003	-0.004	0.004	-0.001	-0.002	0.001	-0.001	-0.004	-0.003	0.000	0.257	0.252	1.957
10	0.003	-0.003	-0.002	-0.002	0.001	-0.006	0.005	-0.004	0.005	-0.002	0.276	0.280	1.278
…	…	…	…	…	…	…	…	…	…	…	…	…	…
118	-0.007	0.028	-0.001	0.008	0.010	-0.006	-0.004	0.016	0.017	0.035	0.541	0.531	1.806
119	0.002	0.004	0.012	0.016	-0.002	-0.032	-0.002	0.018	0.001	0.012	0.481	0.493	2.533
120	-0.011	0.016	0.034	-0.007	0.016	0.005	-0.010	0.011	0.010	0.005	0.532	0.527	0.858
121	0.017	-0.025	0.000	-0.023	0.026	-0.002	-0.008	-0.009	0.002	-0.009	0.586	0.586	0.014
122	0.007	-0.003	-0.013	-0.033	0.019	-0.001	-0.010	-0.024	0.014	0.017	0.604	0.623	3.068
123	0.000	-0.019	0.049	-0.002	-0.010	-0.001	-0.007	0.005	-0.010	0.001	0.760	0.787	3.562
124	-0.031	-0.008	-0.016	0.032	-0.012	0.003	0.023	0.019	-0.023	-0.011	0.747	0.733	1.883
125	-0.017	-0.006	-0.016	-0.003	-0.011	0.010	-0.030	-0.005	-0.042	0.033	0.732	0.756	3.299
126	0.001	0.006	-0.022	-0.043	0.022	0.011	0.036	0.002	-0.008	0.006	0.669	0.679	1.535
127	-0.002	-0.007	-0.033	-0.028	0.027	-0.003	0.009	0.014	0.029	-0.005	0.675	0.682	1.010
128	-0.023	0.006	-0.012	0.037	0.010	-0.031	-0.005	-0.007	-0.031	0.022	0.791	0.754	4.693
…	…	…	…	…	…	…	…	…	…	…	…	…	…
229	0.047	-0.022	-0.054	-0.054	0.025	0.000	-0.040	0.036	0.026	0.018	0.934	0.910	2.618
230	-0.035	0.001	0.060	-0.046	0.034	-0.012	-0.028	-0.008	0.020	0.002	1.077	1.104	2.496
231	0.063	0.005	0.036	-0.053	-0.041	0.035	-0.045	0.057	-0.012	0.018	1.025	0.994	2.952
232	0.014	-0.009	0.008	-0.018	0.016	0.036	-0.028	0.047	-0.012	0.013	0.803	0.806	0.452
233	0.029	0.050	0.039	0.004	0.007	-0.074	-0.030	0.046	-0.012	0.000	0.872	0.904	3.564
234	-0.008	0.017	-0.045	-0.008	0.029	-0.016	0.043	-0.026	-0.005	0.000	0.859	0.822	4.256
235	0.017	0.005	0.004	0.024	0.027	0.049	0.052	-0.030	-0.015	-0.015	0.872	0.914	4.816
236	-0.015	0.070	-0.016	-0.005	0.000	0.002	0.018	-0.005	-0.029	0.025	1.102	1.151	4.442
237	0.028	-0.010	-0.022	0.018	0.045	-0.019	0.053	0.021	-0.015	0.009	0.908	0.882	2.853
238	-0.012	0.023	-0.050	-0.016	-0.014	-0.047	0.030	0.052	0.024	-0.011	0.967	0.969	0.269
239	0.023	0.037	0.019	-0.005	-0.029	-0.053	-0.041	0.019	0.002	0.045	0.850	0.879	3.385

6. Conclusions

With respect to the considerable effect of GDL pressure distribution on the performance of proton exchange membrane (PEM) fuel cells, a methodology based on parameterized finite element analysis (FEA) and an adaptive neuro-fuzzy inference system (ANFIS) was developed to predict contact pressure distribution on the gas diffusion layer due to dimensional errors of bipolar plate ribs. The methodology of the present study can be used to analyze the effect of dimensional tolerances of bipolar plates in PEM fuel cells. In this regard, finite element simulation was used to model the BPP/GDL contact behavior and calculate the

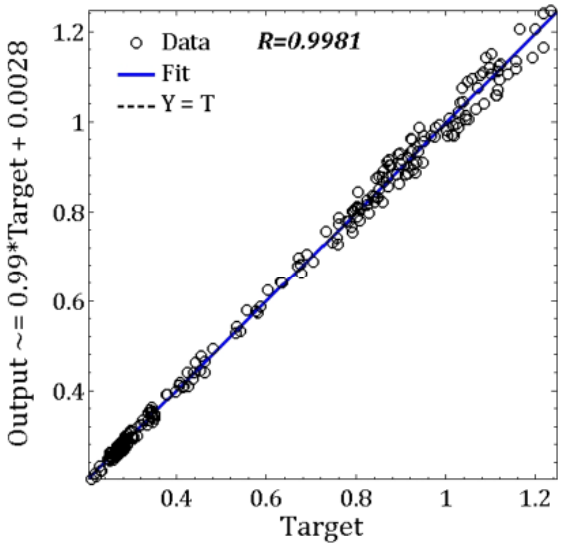

Fig.11. Cross-correlation between estimated and obtained values of Pstd (MPa).

GDL pressure distribution. The numerical results of the finite element solution were experimentally validated. Initially, a range of dimensional tolerances from ±0.01 mm to ± 0.1 mm at an interval of 0.01 mm were modeled with the FEA, respectively, for different combinations of dimensional errors of bipolar plate ribs. Altogether, 270 series of finite element simulations were conducted in this research (10 different tolerances and 27 different combinations of dimensional errors). Then, ANFIS models were successfully trained and tested separately for each dimensional tolerance based on the main data set comprising 27 pairs of ten inputs (combination of dimensional errors of BPP ribs) and one output (standard deviation of the GDL contact pressure). Finally, separate ANFIS models were integrated together for predicting GDL pressure distribution in the whole tolerance range (±0.01 mm to ±0.1 mm). It was demonstrated that the proposed integrated prediction model was feasible and effective for the dimensional tolerances considered. The methodology developed in this study is beneficial in improving the accuracy of BPP and can be applied to guide the manufacturing process for the PEM fuel cell.

References

[1] Hoogers G., Fuel Cell Technology Handbook, CRC Press, Boca Raton, FL, 2003.

[2] Zhou P., Wu C.W. and Ma G.J., "Contact resistance prediction and structure optimization of bipolar plates", J. Power Sources, 2006, 159: 1115.

[3] Zhou Y., Lin G., Shih A.J. and Hu S.J., "Assembly pressure and membrane swelling in PEM fuel cells", J. Power Sources, 2009, 192: 544.

[4] Mishra V., Yang F. and Pitchumani R., "Measurement and Prediction of Electrical Contact Resistance Between Gas Diffusion Layers and Bipolar Plate for Applications to PEM Fuel Cells", J. Fuel Cell Sci. Technol., 2004, 1: 2.

[5] Hasan A.D., Jin S.H. and Joongmyeon B., "Effect of GDL permeability on water and thermal management in PEMFCs – I. Isotropic and anisotropic permeability", Int. J. Hydrogen Energy, 2008, 33: 3767.

[6] Lee W.K., Ho C.H., Van Zee J.W. and Murthy M., "The effects of compression and gas diffusion layers on the performance of a PEM fuel cell", J. Power Sources, 1999, 84: 45.

[7] Andreas V., Kenneth K., Jim D. and Jim S., "Effect of material and manufacturing variations on membrane electrode assembly pressure distribution", In: First international conference on fuel cell science engineering and technology, 2003, Rochester, New York, USA.

[8] Lee S.J., Hsu C.D. and Huang C.H., "Analyses of the fuel cell stack assembly pressure", J. Power Sources, 2005, 145: 353.

[9] Wen C.Y., Lin Y.S. and Lu C.H., "Experimental study of clamping effects on the performances of a single proton exchange membrane fuel cell and a 10-cell stack"; J. Power Sources, 2009, 192: 475.

[10] Zhou P., Wu C.W. and Ma G.J., "Influence of clamping

force on the performance of PEMFCs"; J. Power Sources, 2007, 163: 874.

[11] Bograchev D., Gueguen M., Grandidier J.C. and Martemianov S., "Stress and plastic deformation of MEA in running fuel cell", Int. J. Hydrogen Energy, 2008, 33: 5703.

[12] Tang Y., Kusoglu A., Karlsson A.M., Santare M.H., Cleghorn S. and Johnson W.B., "Mechanical properties of a reinforced composite polymer electrolyte membrane and its simulated performance in PEM fuel cells", J. Power Sources, 2008, 175: 817–825.

[13] Liu D., Peng L. and Lai X., "Effect of dimensional error of metallic bipolar plate on the GDL pressure distribution in the PEM fuel cell", Int. J. Hydrogen Energy, 2009, 34: 990.

[14] Liu D., Peng L. and Lai X., "Effect of assembly error of bipolar plate on the contact pressure distribution and stress failure of membrane electrode assembly in proton exchange membrane fuel cell", J. Power Sources, 2010, 195: 4213.

[15] Lee W.K., Ho C.H., Van Zee J.W. and Murthy M., "The effects of compression and gas diffusion layers on the performance of a PEM fuel cell", J. Power Sources, 1999, 84: 45.

[16] Wang X.T., Song Y. and Zhang B., "Experimental study on clamping pressure distribution in PEM fuel cells", J. Power Sources, 2008, 179: 305.

[17] Yi P.Y., Peng L.F. and Ni J. "A numerical model for predicting gas diffusion layer failure in proton exchange membrane fuel cells", J. Fuel Cell Sci. Technol., 2011, 8: 011011.1.

[18] JANG J.S.R., "ANFIS: Adaptive-Network- Based Fuzzy Inference System", IEEE Trans. Systems, Man and Cybernetics, 1993, 23: 665.

[19] Hagan M.T., Demuth H.B. and Beale M., "Neural Network Design", PWS Publishing Company, Boston, 1996.

[20] The Math Works Inc. Product, 2005, Neural Network Toolbox Version 4.0.1 MATLAB 7.0.1 release 14 service pack 3, The Math Works Inc.